This article has been accepted for publication in a future issue of this journal, but has not been fully edited. Content may change prior to final publication. Citation information: DOI 10.1109/TPWRD.2018.2808428, IEEE Transactions on Power Delivery

Directional, High-Impedance Fault Detection in Isolated Neutral Distribution Grids

Carlos Gonzalez, Jeroen Tant, *Member, IEEE*, Jean Gardy Germain, *Member, IEEE*, Tom De Rybel, and Johan Driesen, *Senior Member*, IEEE.

***Abstract*— This paper presents an algorithm for fast, directional detection of phase-to-ground faults in isolated neutral distribution grids. The method reacts directionally and very fast to fault conditions (1-2 samples after fault inception, even without large di0/dt). Moreover, the method is able to detect low- and High-Impedance Faults (HIF), permanent or transient faults. The algorithm is independent of the sampling frequency, very robust to noise and does not need calibration of the sensors. The direction detection method relies on the fault model identification, based on the zero-sequence grid capacitance estimate for isolated neutral grids. The estimate is obtained from the fault circuit differential equation, solved with the least-squares method, where appropriate numerical modifications have been introduced. The sign of the estimate provides the directional information, whereas the magnitude of the modified estimate indicates the fault. The directional principle is validated in simulation and the fault detection method is validated with real fault records from the RedNA project. The paper re-works the equations that define the Non-Detection Zone, so that the method is comparable to the classical residual over-current and over-voltage functions, typically used to detect HIF.**

***Index Terms*— directional fault detection, isolated neutral grid, High-Impedance Fault (HIF).**

I. Introduction

THE most typical fault type in Medium Voltage (MV) Distribution Grids is phase-to-ground (PTG) fault, accounting for between 70 and 80% of the total number of faults [1]. The grounding impedance limits the fault current in case of single phase-to-ground faults, by increasing the impedance of the earth current return path [2]. In low-impedance grounding systems, phase-to-ground faults can be relatively easily detected because of the large phase and zero-sequence fault current. The current magnitudes are large enough so that only phase current sensors are needed. This is not the case for high-impedance grounding systems, such as isolated neutral systems. The zero-sequence impedance is dominant with respect to the other sequence impedances, yielding very low fault currents, so that the phase currents remain within the normal load current levels. The zero-sequence current and voltage become the most reliable and sensitive magnitudes to trigger the fault detection, typically the ANSI functions 51N, 59N and 67N, in the Sensitive Ground subclass.

Typical threshold values for fault detection are: residual 0,4 A for homopolar over-current and around 2% of the nominal voltage for the homopolar over-voltage. In addition, because of the over-voltage in the healthy phases, the fault detection time has to be fast, in the range of 50 or 60 ms, to protect the cable insulation [3].

The use of zero-sequence magnitude for fault detection becomes a major difference with respect to other grounding systems. In other (low-impedance) grounding systems, directional fault detection relies on phase voltage (and current), leading to problems in case of close-in faults, where the sensors are located very close to the actual fault location. The phase voltage collapses to zero and makes the fault detection less reliable and more complex. Fault detection schemes that work with zero-sequence voltage instead do not experience the close-in fault phenomenon. For similar reasons, zero-sequence magnitudes-based methods are insensitive to reverse power flows that only involve positive or negative sequence currents. Another important issue is the connection of loads. In isolated neutral grids, Low-Voltage (LV) loads are connected to the MV side with a DY transformer connection that blocks any homopolar current influence from the LV to the MV side. Hence, the I0> and U0> functions, and any other method working with homopolar magnitudes, are insensitive to the load homopolar unbalances in the LV side.

The classical directional fault detection is achieved with a zero-sequence voltage polarization scheme [2,4,5], where the polarizing magnitude is the zero-sequence voltage and the operating magnitude is the sensitive zero-sequence current. For isolated neutral grids, the zero-sequence current is almost 90 degrees shifted from the zero-sequence voltage. The sign of the angle shift determines the direction.

An important percentage of phase-to-ground faults are transient or self-extinguishing, that may disappear after few milliseconds [1]. Re-striking faults can reignite around the voltage peak instants. According to the statistics in [1], in isolated neutral grids, the average residual current was 0,9 A, whereas the maximum residual current measured in a fault was 9,5 A.

This work was supported by the KIC-InnoEnergy - Active SubStations project, from the European Institute of Technology (EIT).

C. Gonzalez, J. Tant, T. De Rybel and J.Driesen are with the Department of Electrical Engineering ELECTA/ESAT, Katholieke Universiteit Leuven, Kasteelpark Arenberg 10, bus-2445, Heverlee, B-3001, Belgium.

J.G. Germain is with Gas Natural Fenosa, Avda. San Luis 77, Madrid 28033, Spain.

E-mail: carlos.gonzalezdemiguel@kuleuven.be

This article has been accepted for publication in a future issue of this journal, but has not been fully edited. Content may change prior to final publication. Citation information: DOI 10.1109/TPWRD.2018.2808428, IEEE Transactions on Power Delivery

A. Fault circuit model-based fault detection algorithm

The fault circuit model of Fig. 1 is broadly used to study PTG faults in isolated neutral grids. The model has been simplified assuming the zero-sequence impedance dominate over the positive and the negative impedances. Therefore, this model requires only few parameters: the phase voltage, the circuit zero-sequence capacitance and the fault resistance.

The available real fault records show that measurements follow very closely the model. This observation has become the starting point to propose a fault detection method based on the estimation of the zero-sequence capacitance parameter, obtained from the fault circuit model equations.

If the capacitance estimate falls close to a reasonable grid capacitance value, this will indicate the presence of a fault, regardless of the fault impedance, because the measurements match the model. The estimate is obtained from filtered or unfiltered instantaneous samples and evaluated in real-time. In practice, the exact value of the grid capacitance is usually hard to know and far from constant. The inexact modeling of the grid components, the variable grid topology and the thermal drift of the electrical properties are factors of uncertainty.

As any other detection method, the proposed one also requires a threshold definition. The choice of the estimate threshold is, however, not obvious. The threshold value must be high enough to be insensitive to the small grid imbalances and to the noise in the zero-sequence magnitudes in pre-fault conditions. At the same time, the threshold must be low enough to maximize the detection capabilities. The authors propose a self-configuration algorithm to scale the estimate to fit according to a pre-defined and already known threshold.

B. Directional fault detection

Following the conventional directionality methods (based on quadrature polarization), the sign of the estimate provides fault direction information, as it can be deducted from Fig. 1 (arrow direction of zero-sequence current $I_{0,fwd}$ and $I_{0,rev}$).

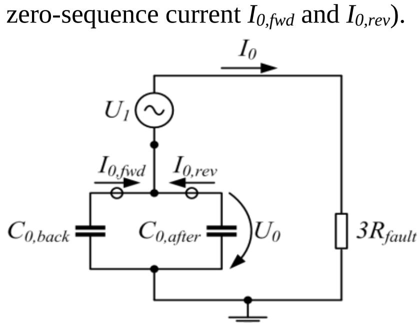

Fig. 1. Simplified sequence scheme for phase-to-ground faults in isolated neutral grids.

U_1 stands for the faulted phase voltage, R_{fault} is the fault resistance, C_0 represents the capacitance before (back) and after the fault. U_0 is the zero-sequence voltage.

Because the zero-sequence capacitance is distributed all over the grid, it is deducted that the homopolar current flows in all the grid branches. Moreover, because the shunt capacitances dominate over the series elements, the zero-sequence voltage is almost constant all over the grid. Therefore, all the grid relays based on zero-sequence over-current (I0>) and zero-sequence over-voltage (U0>) require directionality to discriminate the faulted feeder from the healthy ones, for grid reliability and fast fault location. The dominance of the shunt capacitances also implies that distance relays with homopolar magnitudes are not precise enough in practice.

C. Comparison of Non-Detection Zones

In [3], a fault detection scheme based on I0> and U0> is proposed to tackle HIF-faults. The Non-Detection Zone can be identified as the opposite region of the operation region, as reproduced in Fig. 2.

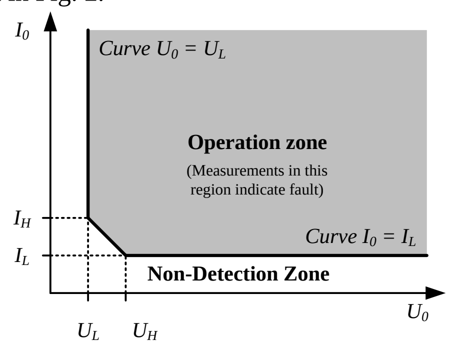

Fig. 2. Operation zone for HIF phase-to-ground faults, according to [3].

The Distribution System Operator (DSO) proposes the indexes H and L for High and Low values, although not always implemented (I_H=I_L and U_H=U_L). The proposed method works with a different principle than the baseline proposed in Fig. 2 [3]. In order to allow comparison of methods, the baseline Non-Detection Zone (NDZ) must be expressed in different terms. We propose to compare the baseline and the estimate method in the C_0-R_{fault} plane. This requires the arrangement of the fault circuit equations derived from Fig. 1, for the zero-sequence voltage and current, replacing U_0 and I_0 by the corresponding thresholds U_L and I_L.

$$R_{fault}(C_0)\Big|_{U_0=U_L} = \frac{\sqrt{U_1^2 - U_0^2}}{3\omega C_0 U_0} \tag{1}$$

$$R_{fault}(C_0)\Big|_{I_0=I_L} = \frac{1}{3\omega C_0} \cdot \sqrt{\left(\frac{U_1 \omega C_0}{I_0}\right)^2 - 1} \tag{2}$$

Where ω is the angular grid frequency [rad/s], and C_0 is total zero-sequence grid capacitance, as the sum of the $C_{0,back}$ and $C_{0,after}$. For simplicity, the authors have omitted the small, triangular Non-Detection Zone framed between I_H, I_L, U_H and U_L in Fig. 2. The arrangement of the equations yields two functions of $R_{fault} = f(C_0)$, that correspond to the U0> and the I0> detection functions and are plotted in Fig. 3. The figure shows the NDZ as well as the operation zone, as the intersection area below the curves-equations (1) and (2).

The left side of Fig. 3 corresponds to low-capacitance grids, mostly formed by OverHead Lines (OHL) and the right side to high-capacitance grids, formed by UnderGround Cables (UGC). Fig. 3 shows the detection function I0>, the function U0> and the combination of both. Representing the fault detection functions in the C_0-R_{fault} plane allows us to conclude that the I0> and U0> functions are unevenly effective (in terms of R_{fault} coverage range). The I0> function allows detecting

This article has been accepted for publication in a future issue of this journal, but has not been fully edited. Content may change prior to final publication. Citation information: DOI 10.1109/TPWRD.2018.2808428, IEEE Transactions on Power Delivery

higher resistance faults in UGC grids, whereas the U0> function is more effective in OHL grids.

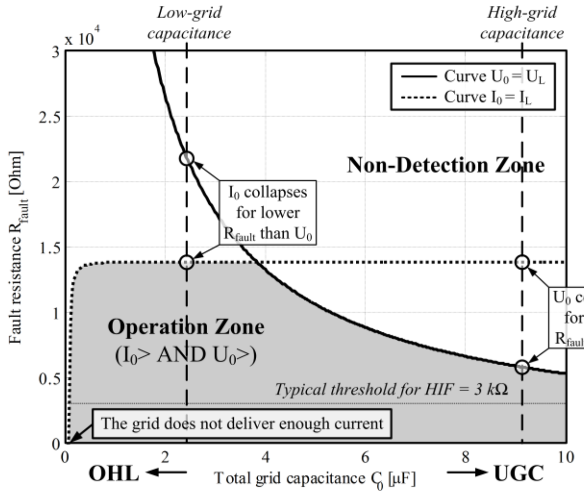

Fig. 3. Equivalent Non-Detection Zone and operation zone of Fig. 2, from [3], expressed in terms of grid capacitance and fault resistance. The gray zone corresponds to the detection (or operation) zone, whereas the white zone corresponds to the NDZ. The combination of U0> and I0> can cope with HIF, above 3 kΩ. The limits of the fault resistance for the I0> and the U0> functions are plotted for different scenarios of grid capacitance (low- and high-grid capacitance).

D. HIF detection

The detection of HIF has been under study since 1970. HIFs have been described as “random behavior with unstable and wide fluctuation in current” [6]. Several papers have collected and classified the broad range of detection methods in literature [7-8], and several publications have shown tests, issues, models and statistics [9-16]. In general terms, the detection methods in literature are based on different analysis techniques to extract features of the HIF, mainly harmonics (spectral content [17-18], wavelet coefficients [19-23]), or more elaborated techniques, such as neural networks [24-25], expert systems [26-27], mathematical morphology [8], or the combination of several algorithms [28-35].

In general, most of these methods have drawbacks in one or more of the following aspects: (i) either they are slow, they require long time windows before detecting the fault, (ii) the detection methods are supervised by a conventional overcurrent function, hence, they incur the same Non-Detection Zone as low-impedance faults, (iii) they require a high sampling frequency, which makes it difficult to implement, for instance, in directional Fault Passage Indicators (FPI), intended to be low-cost devices for large-scale roll-out, (iv) they need calibration and configuration of sensors, hence contributing to the total cost of an FPI solution, for instance, (v) they are not directional or (vi) the configuration of the fault detection parameters is implicitly grid-dependent or without a physical meaning, becoming a burden towards the practical implementation of such methods, or (vii) they are designed only for low-impedance grounding systems. In high-impedance grounding grids, the shunt parameters play a crucial role in phase-to-ground faults, in low impedance fault, but also in HIF.

When it comes to simulation of HIF, many models are proposed, but many of them derived after the Emanuel arc model [11]. These models maintain the two (antiparal·lel) diode-branches, combining either linear or variable resistances and/or variable voltage sources. Another model proposes a Transient Analysis of Control System (TACS) block that controls the opening and closing of the fault switch [22]. A review of different HIF models is summarized in [36]. The ground fault model is applied to the faulted phase.

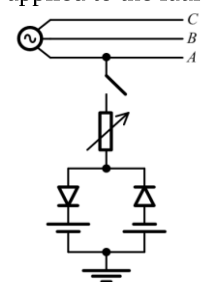

Fig 4. HIF model from [37], consisting of a variable resistance and two diodes with DC voltage sources in series.

Because faults in isolated respond so close to the fault model and concern only the zero-sequence magnitudes, the scheme of Fig. 4 can be re-drawn similarly as in Fig. 1, where the fault resistance is replaced by the HIF model. The switch has been removed; it is implicitly included in the fault model.

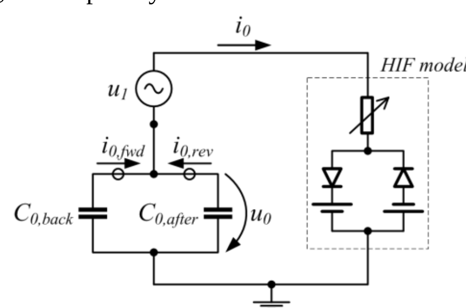

Fig 5. The HIF model can be embedded in the sequence fault model, showing how detection methods with instantaneous homopolar magnitudes are immune to the fault resistance model, even in dynamic situations.

This paper proposes a fault detection method that tackles all the drawbacks mentioned previously: fast fault detection, HIF detection capabilities, suitable for isolated neutral grids, directional, able to cope with arcing faults, implementable with low sampling frequencies and easy to calibrate. On top of these features, the proposed method aims to maximize the fault detection capabilities that arise from the preliminary analysis of the NDZ, either in low or high grid capacitances.

Section II includes a description of the fault detection method, from the calculation of the estimate, the self-calibration of the threshold and the noise influence. The detection method is validated with real fault records from the RedNA project in section III. Section IV concludes the paper and discusses some issues related.

II. Fault Detection Principle

In general, the zero-sequence parameters of the circuit are difficult to calculate offline because of the multiple factors influencing the value, such as the geometry of the OHL poles and conductors, the type of cables and insulation, their lengths,

This article has been accepted for publication in a future issue of this journal, but has not been fully edited. Content may change prior to final publication. Citation information: DOI 10.1109/TPWRD.2018.2808428, IEEE Transactions on Power Delivery

temperature and many more. Instead, parameter estimation is used for calculations. For isolated-neutral grids, estimating the capacitance can be done with the imaginary part of the impedance with the 50 Hz components. Estimating the impedance takes one electrical period, which is almost half of the detection time. A faster method can be implemented with the Differential Equation Algorithm (DEA), which has been successfully applied for fast fault detection and distance calculations, amongst other applications [38,39] and that helps coping with the unpredictable and random behavior of HIF faults. The zero-sequence capacitance is estimated from:

$$i_0 = C_0 \frac{du_0}{dt} \tag{3}$$

Integration of (3) leads to

$$\frac{1}{C_0}\int i_0 dt = \int du_0 \tag{4}$$

Equation (4) is integrated with the trapezoidal method, used frequently in other DEA applications. Hence, obtaining a capacitance estimate every discrete time instant k, being Δt the time step ($\Delta t = 1/Fs$) and Fs, the sampling frequency:

$$\frac{\Delta t}{2}\cdot\frac{1}{C_{0,k}}\cdot\left(i_{0,k}+i_{0,k-1}\right)=\left(u_{0,k}-u_{0,k-1}\right) \tag{5}$$

Rearranging the terms of (5), C_0 can be estimated by:

$$C_{0,k} = \frac{\Delta t}{2}\cdot\frac{i_{0,k}+i_{0,k-1}}{u_{0,k}-u_{0,k-1}} \tag{6}$$

Depending on the fault location, the algorithm estimates the capacitance upstream (left) or downstream (right). The sign of the capacitance estimate provides directional information. According to the change of sign of the zero-sequence voltage, shown in Fig. 1, a positive-sign capacitance indicates reverse direction, whereas negative-sign indicates forward fault direction. The absolute value has to be taken for grid parameter estimation purposes or a plus/minus threshold.

However, (6) is badly conditioned in specific cases: when the zero-sequence voltage waveform reaches the positive or negative peaks, the voltage increment is almost zero, leading to abnormally high values of capacitance. This drawback has been minimized by using a vector of n samples and the Least Squares (LS) Method to solve the system.

$$\frac{\Delta t}{2}\cdot\begin{bmatrix} i_{0,1}+i_{0,0} \\ i_{0,2}+i_{0,1} \\ \vdots \\ i_{0,n}+i_{0,n-1}\end{bmatrix} = \begin{bmatrix} u_{0,1}-u_{0,0} \\ u_{0,2}-u_{0,1} \\ \vdots \\ u_{0,n}-u_{0,n-1}\end{bmatrix}\cdot C_{0,n} \tag{7}$$

One particular case of fault is the re-striking type, where the fault ignites, disappears and strikes back again few instants later. Normally, the re-ignition of the fault takes place around the voltage peak, either maximum or minimum. For this reason, it is of special interest to calculate the estimate with vectors long enough, so that in every division there is one voltage peak/valley represented in the vector. This will guarantee that, when the fault ignites, regardless of the time instant, the estimate reflects the fault occurrence almost immediately. Therefore, n is sized to be half electrical period, $n=Fs/(2\cdot Fg)$, where Fg is the grid frequency. Equation (7) can be used with nearly any sampling frequency, above Nyquist criteria, although reasonable values are higher than 800 Hz.

The Least-Squares method solves a problem of the type

$$b = B\cdot C_0 \tag{8}$$

Where B is the voltage-term vector, b is the current-term vector. Under certain conditions, it is possible that the zero-sequence capacitance is around zero in pre-fault conditions. Implementing a straightforward detection method based on the increment of the estimate with respect to the pre-fault estimate is not a suitable method.

In an ideal situation (the grid is perfectly balanced and perfect sensors), in pre-fault conditions, residual current and voltage are zero. Therefore, the use of the estimates for fault detection purposes leads to an undetermined division of $0/0$. In real conditions, there are several unbalances that can take place: grid unbalances in capacitances, the sensors have an error in the measurements and there is noise in the signals. These deviations may not yield a $0/0$ undetermined division, but they can largely affect the estimate in pre-fault conditions, providing an unreal grid estimate.

On top of this, the model introduced in Fig. 1 describes the behaviour of the zero-sequence magnitudes (i_0 and u_0) during fault conditions, but cannot be applied in pre-fault conditions. It is expected, however, that the grid unbalances lead to small zero-sequence voltages and currents. In the case of the residual current, because of the very small currents to be detected, the pre-fault measurements can be in the order of magnitude of the quantization steps of an Analog-to-Digital Converter (ADC).

Altogether, this implies that the pre-fault estimate is a mix of all these factors and cannot be applied straightforward and trusted for fault detection purposes.

A. *Modification of the estimate*

In order to overcome the non-determined division, it is proposed to add a term α, large enough, to (8), becoming:

$$C_{0,\text{mod}} = \left(B+\alpha\right)\backslash b \tag{9}$$

so that the division is no longer undetermined, forcing the $C_{0,mod}$-estimate to be a very small value, close to 0 in pre-fault conditions. Note that the new estimate is no longer C_0, but $C_{0,mod}$, meaning that the estimate is no longer a parameter describing the grid capacitance, although closely related.

The term α can be a constant value or a vector, of a specific signal type or noise. For directional detection purposes, it is crucial to preserve the sign of the estimate. Therefore, it is required the term α to be a vector of 0-mean value. For simplicity, the preferred signal is a triangular saw-tooth function of the highest frequency possible, $Fs/2$, being Fs the sampling frequency, between $\{-1; 1\}$, as shown in Fig. 6. The signal will be later scaled with the factor A.

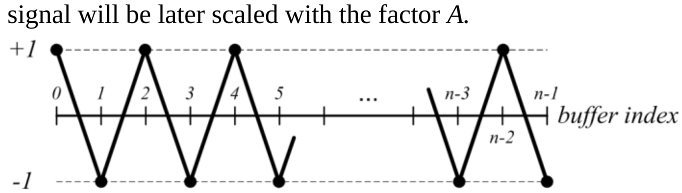

Fig 6. Tooth-saw signal s_1, starting with $+1$, the inverse signal is $s_2 = -s_1$.

Solving the DEA equation with Least-Squares technique, for instance, will try to fit any capacitance to the model, no matter the frequency. That means that the estimate will respond to the grid frequency (50 Hz) as well as the saw-tooth frequency and other frequencies present in the signals, for instance, the cable discharge frequency or the 150 Hz ferro-resonance frequency (when the fault is cleared).

The cable discharge current and the 50 Hz grid current frequencies are useful for the estimate, whereas the ferro-resonance currents, at 150 Hz, and the saw-tooth frequency content should be removed from the estimate. The ferro-resonance of 150 Hz will be left out of the scope, since it only takes place after the fault is cleared and has a short duration (maximum of 2 periods) and a small magnitude.

In the next subsections, a distinction will be made between the polarity of both sequences s_1 (first peak is positive) and s_2 (first peak is negative). Equation (9) becomes:

$$C_{0,\mathrm{mod},s1} = \left(B + A\cdot s_1\right)\backslash b \tag{10a}$$

$$C_{0,\mathrm{mod},s2} = \left(B + A\cdot s_2\right)\backslash b \tag{10b}$$

upon the chosen sequence, where A is the amplitude of the saw-tooth signal. Finding the right amplitude A becomes of major importance in this application. The addition of the terms $A{\cdot}s_1$ and $A{\cdot}s_2$ introduces a $Fs/2$ ripple in the estimate that is mitigated by averaging $C_{0,mod,s1}$ and $C_{0,mod,s2}$, becoming $C_{0,avg}$. In case $||b||$ and $||B||$ are 0, the estimate is 0, by definition.

B. Determining the amplitude A (pre-fault scenario)

The underlying idea is to force the pre-fault estimate ($C_{0,avg}$) to be a very low value, around 0. We pre-define τ as the boundary for the estimate, so that ($-\tau \le C_{0,avg} \le \tau$). The zero-sequence grid capacitance is in the order of magnitude of tens of μF [38]. After numerical transformation of the estimate, τ is not a dimensional parameter, but *comparable* to a very small value of capacitance, few nF. A suitable value is $\tau = 3{\cdot}10^{-9}$.

In order to force the pre-fault estimate below τ, the method requires a pre-fault configuration time to characterize the fluctuations of the estimate and determine the best value for the amplitude A. The formulation of the LS-method minimizes the error function $f(C_{0,avg})$, which can be written as

$$\min_{C_{0,avg}} f(C_{0,avg}) = \left\| B^T B{\cdot}C_{0,avg} - nA^2 C_{0,avg} - b^T B \right\|_2 \tag{11}$$

Given that $C_{0,avg}$ is constrained within the limits of τ, (11) can be written as in (12), replacing $C_{0,av}$ by τ or $-\tau$. The problem becomes minimizing the error function depending on $A{:}f(A)$.

$$\min_{A} f(A) = \left\| \pm B^T B{\cdot}\tau \mp nA^2\tau - b^T B \right\|_2 \tag{12}$$

The minimization of the 2-norm responds to

$$\frac{df(A)}{dA} = 0 \tag{13}$$

Equation (12) is expanded and derived, according to (13), so that the amplitude A is calculated as

$$A^2 = \max\left\{ \frac{\pm\tau B^T B \pm b^T B}{n\tau} \right\} \tag{14}$$

Fig. 7 shows the zero-sequence voltage, current and the calculated parameter A in pre-fault situation, according to (14) from real fault records in two different grids with isolated neutral. It can be seen that impedance-balanced grids show small, pre-fault zero-sequence voltage and current.

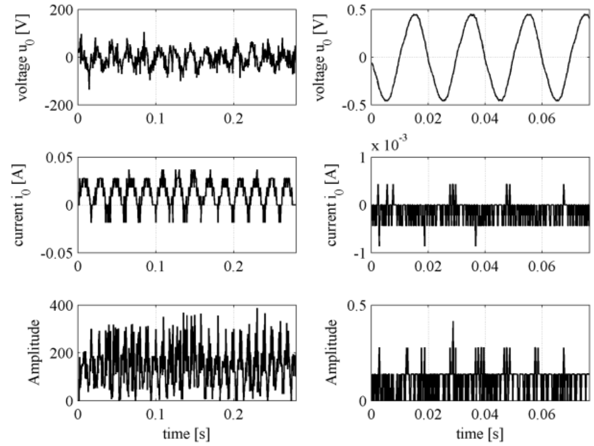

Fig 7. Zero-sequence voltage (u_0), zero-sequence current (i_0), calculated amplitude (A-parameter), during pre-fault conditions. (a) High grid impedance unbalance. (b) Low grid impedance unbalance. The more unbalance in the grid capacitance, the larger the amplitude, forcing the pre-fault capacitance to be close to a 0-value.

Given the maximum amplitude, the threshold can be automatically set up at a slightly higher value that allows to cope with noise and imbalance variations, and still guarantees maximizes the operation zone of the method. The authors propose:

$$\tau_{threshold} = 1.5\times\tau = \pm 4.5{\cdot}10^{-9} \tag{15}$$

The threshold applies for both the positive and the negative estimates. By doing this, the method self-adjusts the detection threshold to the estimate. The estimate usually reaches values very small, around the *micro*- and *pico*-units. This can be seen as a numerical challenge in practical implementations. These concerns imply using specific number types, such as *float* or *double precision float* numbers and corresponding operations.

C. Noise and harmonics influence

Up to now, the method has been introduced without considering the effect of the noise or harmonics on the measurements and the estimate. Still, the detection principle is able to cope with filtered as well as with unfiltered samples. However, for the sake of clarity, the effect of noise and harmonics is explained next. We consider harmonics and noise both in the current and voltage measurements. There exist many sources of noise and models to study it. However, it is not the scope of the paper to discuss them. Here, the noise has been modelled as random samples with limited amplitude superimposed to the voltage and current signals (σ_i and σ_u). A sample k of current and voltage with harmonics (as a Fourier sinus-series) and noise is notated as

$$i_{0,k} = i_{0,DC} + \sum_{m=1}^{T} C_{i,m}\cdot\sin\left(2\pi\frac{m\cdot F_g}{F_s}k + \varphi_{i,m}\right) + \sigma_i \tag{16a}$$

$$u_{0,k} = u_{0,DC} + \sum_{m=1}^{T} C_{u,m}\cdot\sin\left(2\pi\frac{m\cdot F_g}{F_s}k + \varphi_{u,m}\right) + \sigma_u \tag{16b}$$

Where m is the harmonic index, C and φ are the amplitude and phase angle of the harmonic m waveform and the sub-indexes i or u distinguish the notation for current or voltage, whereas the sub-index *DC* relates to the zero-frequency term. Recall (5), the current samples between two consecutive steps are summed, whereas the voltage samples are subtracted. After manipulation, the sum and the subtraction yield to:

$$i_{0,k} + i_{0,k-1} = \\ = 2\left[\sigma_i + i_{0,DC} + \sum_{m=1}^{T} C_{i,m} \cdot \cos(R)\sin\big(R(2k-1) + \varphi_{i,m}\big)\right] \tag{17a}$$

$$u_{0,k} - u_{0,k-1} = \\ = 2\left[\sigma_u + \sum_{m=1}^{T} C_{u,m} \cdot \sin(R)\cos\big(R(2k-1) + \varphi_{u,m}\big)\right] \tag{17b}$$

Being

$$R = \pi \frac{m \cdot F_g}{F_s} \tag{18}$$

assuming that the DC term, the amplitude *C* and the angles φ do not change from sample (k-1) to k. Recall the calculation of the estimate from (6), without the modifications introduced by parameter *A*, the development of (17a) and (17b) leads to

$$C_{0,k} = \frac{\Delta t}{2} \cdot \frac{\sigma_i + i_{0,DC} + \sum_{m=1}^{T} C_{i,m} \cdot \cos(R)\sin\big(R(2k-1) + \varphi_{i,m}\big)}{\sigma_u + \sum_{m=1}^{T} C_{u,m} \cdot \sin(R)\cos\big(R(2k-1) + \varphi_{u,m}\big)} \tag{19}$$

From (19), it can be deducted how the DC offset in the current signal plays an important role in the estimate, both in pre-fault or fault conditions. Therefore, the implementation of the method in practice will require blocking the DC term. Regarding the voltage, the DC offset cancels out with the subtraction operation. In fault conditions, the harmonics of both the current and the voltage are related to each other, following the capacitive circuit of Fig. 1. Recall the arrow direction of the currents signals, which implies that the angles φ_i and φ_u are delayed $\pm\pi/2$ upon the fault direction.

Consider the trigonometric identity

$$\sin\left(\frac{\pi}{2} - \alpha\right) = \cos\alpha \tag{20}$$

to illustrate how each harmonic of the current and the voltage will be in phase (*0* radians delay) or out-of-phase (π radians delay) upon the fault direction. Therefore, including the harmonics in the calculation of the estimate can reinforce the directional feature of the proposed method. Still, given the superposition of the many terms in (19), it is not trivial identifying how the harmonics will precisely influence the estimate. The harmonics of the current can boost the value of the estimate, whereas the harmonics of the voltage will reduce the estimate value.

Regarding the influence of the noise, for the sake of clarity, the harmonics will be neglected in equations. Given the inherent uncertainty of the noise sample, the calculations are done with the worst-case scenario, where the noise takes the most extreme value, upon the operation. Hence, (6) becomes

$$C_{0,k} = \frac{\Delta t}{2} \cdot \frac{i_{0,k} + i_{0,k-1} \pm 2\sigma_i}{u_{0,k} - u_{0,k-1} \pm 2\sigma_u} \tag{21}$$

From (21) it can be deducted that the larger the noise in the voltage signal, the smaller the estimate. In a similar way, the noise in the current measurement also has a direct impact on the estimate. However, it is expected that the current measurement is less noisy, given that in isolated neutral grids, the homopolar current is measured with a sensitive residual current sensor, whereas the homopolar voltage is often obtained with the arithmetic sum of the three phase-to-ground voltages, yielding a compound error term.

When analysing the pre-fault conditions, let's consider the balanced scenario, where there measurements only contain noise, no grid-based signal, so that (21) can be written as:

$$C_{0,n,pre-fault} = \pm \frac{\Delta t}{2} \cdot \frac{\sigma_i}{\sigma_u} \tag{22}$$

Therefore, the amplitude *A* must compensate for this, and is calculated from (14), as worse case scenario:

$$A = \sqrt{4n \cdot \sigma_u^2 + \frac{2n\Delta t}{\tau} \cdot \sigma_i \sigma_u} \tag{23}$$

When computing the LS-method as in (10a, 10b), the terms *b* and *B* will be affected by the noise, yielding, most likely, a larger value of *A* than without noise. This will reduce the estimate magnitude, hence compromising the detection capabilities of the method.

D. *Simulations of noise*

Recall the C_0-R_{fault} plane of Fig. 3. For each pair (C_0, R_{fault}), we have calculated the zero-sequence current and voltage amplitude from the fault circuit of Fig. 1, considering a line voltage of 12 kV, neglecting the harmonics and other effects, only 50 Hz. Each leads to one scenario of homopolar current and voltage. For each scenario, some noise has been added on top of the current and voltage signals. The amplitude of the current and the voltage noise has been increased. For simplicity, we restrict the possibilities by relating the amplitude of the current noise with the amplitude of the voltage noise as follows

$$\sigma_u = \frac{U_L}{I_L} \cdot \sigma_i \tag{24}$$

where U_L and I_L are the lower voltage and current thresholds from Fig. 2. No harmonics have been included in the simulations, only the 50 Hz component. The amplitude *A* has been obtained from 5 electrical periods of pre-fault signal, where only the noise is measured. In order to minimize the influence of randomness of the noise, we have run 100 simulations for each scenario with the random noise.

Figure 8 plots in grey scale the percentage of scenarios, out of the 100 simulations, where the fault was detected. Three cases have been included: low, medium and high noise. The black region corresponds to 100% of detected cases (operation zone), whereas the white region and the grey gradient corresponds to the NDZ (none or only few cases were detected). The simulations are compared to the baseline detection method (U0> and I0>), recall Fig. 3, and is represented here by the inner area inside the solid, grey line.

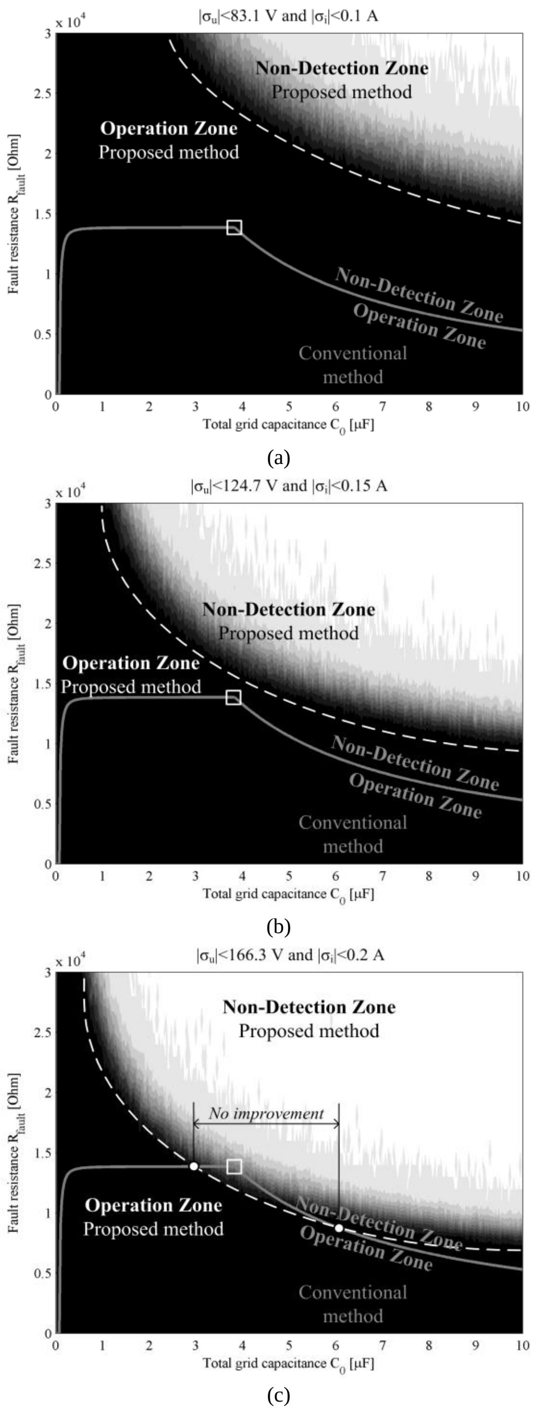

Fig 8. Operation Zone and Non-Detection Zone of the proposed method, compared with the conventional method (I0> and U0>). The solid, gray line shows the detection limit of the conventional method, whereas the white, dashed line represents the approximate limit of the proposed method. The performance is evaluated under different noise levels. (a) Low-level, (b) Medium-level, (c) High-level.

The white square in Fig. 8 represents the intersection point of U0> with I0> functions. The (C_0, R_{fault})-scenario is chosen to illustrate the current and voltage waveforms where the noise has been added. The simulated waveforms, the quantity of noise and the evolution of parameter A have been plotted in Fig. 9, for the three noise levels.

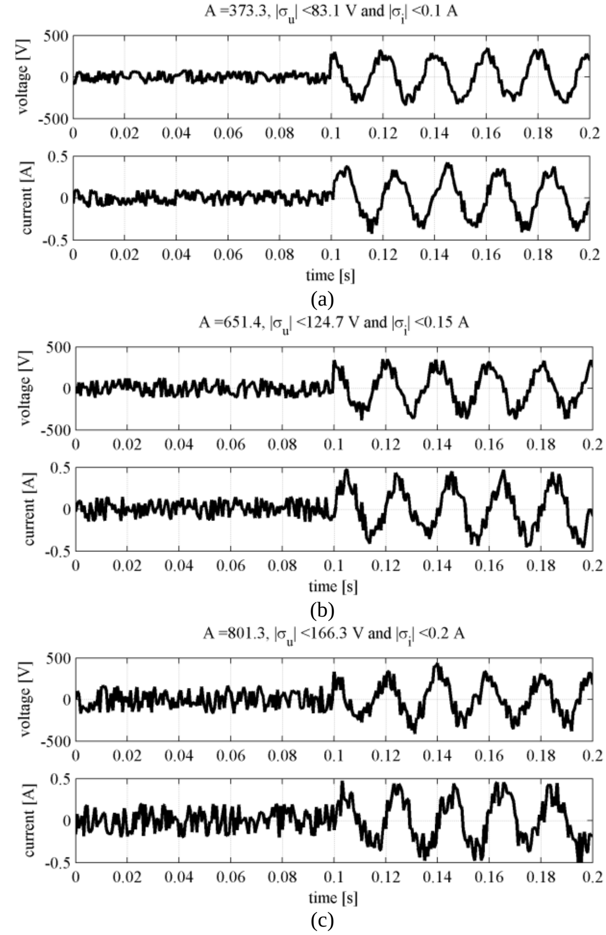

Fig 9. Simulated fault waveforms under different noise levels. (a) Low-level, (b) Medium-level, (c) High-level. The value of the parameter A is forced to increase as the noise amplitude increases.

The simulations reveal that the higher the noise, the larger the NDZ. However, for low- and medium-level noise, the method outperforms regardless of the grid capacitance, overcoming the limitations of the U0> and the I0> functions described earlier. For high levels of noise, the method improves the fault detection capabilities, but only in the extreme cases of very low or very high grid capacitance. Still, regardless of the low-, medium- and high-level classification, the low-level is still a lot of noise, given the low magnitude of the conventional detection thresholds (U_L=138 V and I_L = 0.17 A). For comparison, check the waveforms in Fig. 7.

Moreover, despite the method is robust to the noise influence, it does not imply that the method cannot be implemented with filtered magnitudes. An appropriate filter would likely improve the results, as far as it preserves the phase angle between the voltage and the current. The design of such filter is left out of the scope of the paper.

III. Test Cases

The fault records to validate the method have been obtained from Gas Natural Fenosa (GNF), a large Spanish DSO operating isolated-neutral distribution grids, and E.ON, within the context of the RedNA project. Several faults were created at different test sites (Toranzo and Illescas) with mostly

This article has been accepted for publication in a future issue of this journal, but has not been fully edited. Content may change prior to final publication. Citation information: DOI 10.1109/TPWRD.2018.2808428, IEEE Transactions on Power Delivery

overhead conductors and with different conditions, such as solid fault, resistive faults, on stone, on dry vegetation or trees. For this purpose, a dedicated setup was created to, first, adjust the fault conditions without supply, and then activate the fault during 2 seconds. The practical setup is shown in Fig. 10.

Fig 10. Real fault setup in Toranzo, to create and activate faults in a controlled way. (left) Cable end to arrange the fault conditions. (right) Switching cabin to remotely activate the fault.

The HIF faults were obtained after lowering the thresholds U_L and I_L below the conventional values. The faults were recorded with a sampling frequency of 7200 Hz. We plot the zero-sequence magnitudes in Fig. 11 (a,b,c), as well as the estimate with the corresponding thresholds to prove (i) the fast fault detection and (ii) the directionality. The figures zoom in around the fault inception instant.

Given that the estimate is computed with s_1 and s_2, the estimate achieves very small values in pre-fault conditions. Then, at the fault inception time instant, the estimate reacts very fast, especially if the zero-sequence voltage varies from the expected, pre-fault value.

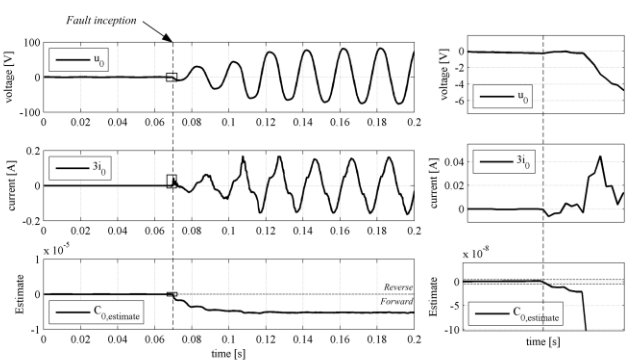

(a)

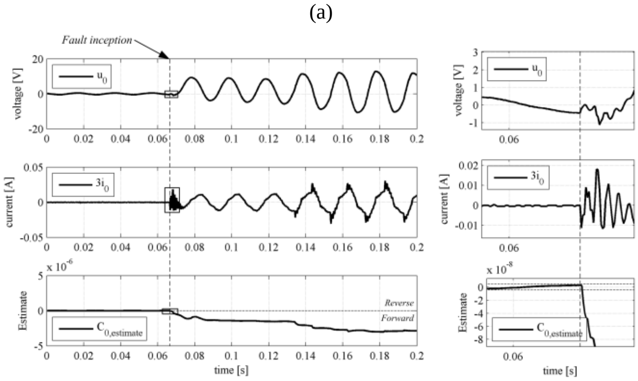

(b)

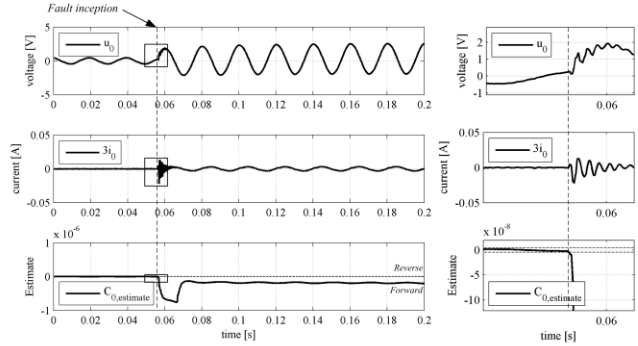

(c)

Fig 11. Real fault records, forward direction, (a), (b) and (c), increasing the fault resistance. Left: Zero-sequence voltage, current and capacitance estimate. Right: zoom around the fault inception time instants to show the fast directional fault detection.

Based on the pre-fault measurements, the amplitude A has been calculated, maximizing the detection capabilities of the method. The results from the test cases indicate that the method reacts very fast to the fault condition, providing directional information equally fast.

IV. Conclusion

This paper has introduced a novel method to detect High-Impedance Faults, very fast and directionally, in isolated neutral grids. The method is based on estimating the zero-sequence grid capacitance and is compared with the conventional one, that uses the U0> and I0> functions. The paper has adapted the Non-Detection Zone (NDZ) of the conventional method in terms of grid capacitance and fault resistance, so that both methods are comparable. Re-writing the NDZ in such terms shows how the performance of the U0> function does not always follow the I0> function, and the way around, depending on the grid capacitance and the thresholds.

The HIF detection method works with the zero-sequence measurements and applies several transformations to improve several aspects of the conventional relays.

A. *Fast Fault Detection*

The fault is soon detected after inception, usually 1 or 2 samples after inception, even when the instantaneous residual current and voltage are small. This makes the method very convenient for fast fault detection, even transient fault detection. In addition, the method can be implemented with nearly any sampling frequency, preferably above 800 Hz. Choosing a low frequency would eventually hide the high-frequency current discharge and other harmonics that can be helpful for the directional detection method.

B. *High-Impedance Fault Detection*

The way the estimate is calculated does not reflect the real grid capacitance, but a parameter with similar characteristics. This is due to the numerical transformations of the actual measurements, but also because the estimate contains the harmonics of the voltage and current. Using LS to obtain the estimate is an advantage because arcing and self-extinguishing faults tend to have high-frequency harmonics and spikes.

C. Self-calibration

The principle of self-calibration consists of encapsulating the pre-fault grid parameter estimate into a default value τ, very close to zero. Given that τ is pre-defined off-line, it does not require prior knowledge of the grid topology. The parameter A is calculated accordingly in pre-fault conditions to adjust to the noise and unbalances.

Still, the threshold from (15) leaves some margin to variations of any type, such as grid topology changes, grid voltage increase or noise variations.

D. Harmonics and noise-robustness

Regarding the influence of harmonics and noise on the performance, the method is robust to reasonable noise levels, above the typical noise levels from the real fault records. The noise in the voltage signal plays a direct role in the estimate and parameter A. Still, the method is able to work with and without filters. The presence of harmonics can reinforce the directionality of method, but the influence on the estimate remains unclear.

V. Further Work

The algorithm has been introduced only for isolated neutral grids. Both the simulations and the test results yield good results, regarding directionality, detection speed and self-calibration. The same method could potentially be applied to other grounding grids where phase-to-ground faults behave closely to the zero-sequence impedance fault model, for instance resonant or compensated neutral or high-resistance grounding. Several adaptations would be required: estimating another parameter than the capacitance, formulating the corresponding DEA, the calculation of parameter A or eventually retuning the value of τ and threshold.

Acknowledgement

The authors of this paper wish to thank Eva Alvarez, Miguel Garcia, Fernando Garcia and Jose Manuel Roca from Gas Natural Fenosa for their collaboration in the KIC-Active SubStations project and the RedNA project.

References

[1] S. Hänninen, "*Single phase earth faults in high impedance grounded networks Characteristics, indication and location,*" Ph.D dissertation, VTT Technical Research Centre of Finland, VTT Publications 453, Espoo, 2001.

[2] N. Fischer, Daqing Hou, "*Methods for detecting ground faults in Medium-Voltage distribution power systems,*" White Paper, *Tech. Report*. SEL, 2006.

[3] Purificacion Lozano et al, *Habitual Practices Used by Spanish Electrical Companies to Deal with High Impedance Faults*, 18th International Conference on Electricity Distribution (CIRED), 2005.

[4] Jeff Roberts, Hector J. Altuve, and Daqing Hou, "*Review of Ground Fault Protection Methods for Grounded, Ungrounded and Compensated Distribution Systems*," Schweitzer Engineering Laboratories, Inc. Pullman, WA USA, 2001.

[5] Jeff Roberts, Normann Fischer and Bill Fleming, "*Obtaining a Reliable Polarizing Source for Ground Directional Elements in Multisource, Isolated-Neutral Distribution Systems,*" White Paper, *Tech. Report*. SEL, 2003.

[6] PSRC Working Group D15, "*High Impedance Fault Detection Technology,*" Report of PSRC. March 1, 1996.

[7] M. Sedighizadeh, A. Rezazadeh, N. I. Elkalashy, "*Approaches in High Impedance Fault Detection - A Chronological Review*," Advances in Electrical and Computer Engineering, vol. 10, 2010, pp. 114 – 128.

[8] S. Gautam and S. M. Brahma, "*Detection of High Impedance Fault in Power Distribution Systems Using Mathematical Morphology*," in IEEE Transactions on Power Systems, vol. 28, no. 2, pp. 1226-1234, May 2013.

[9] B. M. Aucoin and B. D. Russell, "*Distribution High-Impedance Fault Detection Using High-Frequency Current Components*," IEEE Transactions on Power Delivery, Vol. PAS-101, No. 6, 1982, pp. 1596-1606.

[10] B. M. Aucoin and R. H. Jones, "*High impedance fault detection implementation issues*," in IEEE Transactions on Power Delivery, vol. 11, no. 1, pp. 139-148, Jan 1996.

[11] G. A. E. Emanuel, D. Cyganski, J. A. Orr, S. Shiller and E. M. Gulachenski, "*High Impedance Fault Arcing on Sandy Soil in 15 kV Distribution Feeders: Contributions to the Evaluation of the Low Frequency Spectrum*," IEEE Transactions on Power Delivery, Vol. 5, No. 2, 1990, pp. 676-686.

[12] R. Lee and M. Bishop, "*A comparison of measured high impedance fault data to digital computer modeling results*," IEEE Trans. Power App. Syst., vol. PAS-104, no. 10, pp. 2754–2758, Oct. 1985.

[13] S. R. Nam, J. K. Park, Y. C. Kang and T. H. Kim, "*A modeling method of a high impedance fault in a distribution system using two series time-varying resistances in EMTP*," 2001 Power Engineering Society Summer Meeting. Conference Proceedings (Cat. No.01CH37262), Vancouver, BC, Canada, 2001, pp. 1175-1180 vol.2.

[14] Adly. A. Girgis, Wenbin. Chang, Elham. B. Makram, "*Analysis of high-impedance fault generated signals using a Kalman filtering approach*," IEEE Trans. Power Delivery, Vol. 5, No. 4, Nov1990, pp.1714-1724.

[15] N. I. Elkalashy, M. Lehtonen, H. A. Darwish, A-M. I. Taaleb and M. A. Izzularab, "*Feature Extraction of High impedance arcing Faults in Compensated MV Networks. Part I: DWT-Based Analysis of Phase Quantities*", IEEE Power Engineering Society Conference and Exposition in Africa, Power Africa '07,16-20 July 2007, pp. 1-6.

[16] S. Hänninen, M. Lehtonen, U. Pulkkinen, "*A probabilistic method for detection and location of very high resistive earth faults,*" *Electric Power Systems Research*, vol. 54, no. 3, pp. 199-206, Jun. 2000.

[17] A. Ghaderi, H. A. Mohammadpour, H. L. Ginn and Y. J. Shin, "*High-Impedance Fault Detection in the Distribution Network Using the Time-Frequency-Based Algorithm*," in IEEE Transactions on Power Delivery, vol. 30, no. 3, pp. 1260-1268, June 2015.

[18] T. M. Lai, L. A. E. Lo and D. Sutanto, "*High-Impedance Fault Detection Using Discrete Wavelet Transform and Frequency Range and RMS Conversion*," IEEE Transactions on Power Delivery, Vol. 20, No. 1, 2005, pp. 397-407.

[19] M. Michalik, W. Rebizant, M. Lukowicz, Seung-Jae Lee and Sang-Hee Kang, "*High-impedance fault detection in distribution networks with use of wavelet-based algorithm*," in IEEE Transactions on Power Delivery, vol. 21, no. 4, pp. 1793-1802, Oct. 2006.

[20] C. H. Kim, H. Kim, Y. Ko, S. H. Byun, R. K. Aggarwal and A. T. Johns, "*A Novel Fault-Detection Technique of High-Impedance Arcing Faults in Transmission Lines Using the Wavelet Transform*," IEEE Transaction on Power Delivery, Vol. 17, No. 4, 2002, pp. 921-929.

[21] A. R. Sedighi, M. R. Haghifam, O. P. Malik and M. H. Ghassemian, "*High impedance fault detection based on wavelet transform and statistical pattern recognition*," in IEEE Transactions on Power Delivery, vol. 20, no. 4, pp. 2414-2421, Oct. 2005.

[22] D.C. Chan, T. Wai and X. Yibin, "*A novel technique for high impedance fault identification*," IEEE Transactions on Power Delivery, vol. 13, No. 3, pp. 738-744, 1998.

[23] L. L. Lai, E. Styvaktakis, A. G. Sichanie, "*Application of discrete wavelet transform to high impedance fault identification*", IEEE Transactions on Power Delivery, Vol.2, pp. 689-693, 1998.

[24] M. Michalik, M. Lukowicz, W. Rebizant, S. J. Lee and S. H. Kang, "*New ANN-Based Algorithms for Detecting HIFs in Multigrounded MV Networks*," in IEEE Transactions on Power Delivery, vol. 23, no. 1, pp. 58-66, Jan. 2008.

[25] Jae-Ho Ko, Jae-Chul Shim, Chang-Wan Ryu, Chan-Gook Park, Wha-Yeong Yim, "*Detection of high impedance faults using neural nets and chaotic degree,*" International Conference on Energy Management and Power Delivery, 1998.

[26] Ruz, F., and Fuentes, J.A. "*Fuzzy decision making applied to high impedance fault detection in compensated neural grounded MV distribution systems*". Proc. of 7th IEE Int. Conf. on Developments in Power System Protection, 2001, pp. 307-310.

[27] Y. Sheng and S. M. Rovnyak, "*Decision tree based methodology for high impedance fault detection*," IEEE Transactions on Power Delivery, vol. 19, no. 2, pp.533-536, 2004.

[28] T. Baldwin, F. Renovich and L. Saunders. "*Directional ground-fault indicator for high-resistance grounded systems*". IEEE Transactions on Industry Applications. Vol. 39 Nº 2, pp. 325-332. March/April 2003.

[29] Tao Cui, Xinzhou Dong, Zhiqian Bo, Juszczyk, A, "*Hilbert-Transform-Based Transient/Intermittent Earth Fault Detection in Non-effectively Grounded Distribution Systems,"* IEEE Transactions on Power Delivery, vol.26, no.1, pp.143,151, Jan. 2011.

[30] C. Dzienis, M. Kereit, A. Stucker, "*Fault localization in medium voltage networks with compensated and isolated star-point grounding,*" *Modern Electric Power Systems (MEPS), 2010 Proceedings of the International Symposium*, vol., no., pp.1,6, 20-22 Sept. 2010.

[31] S. Sahoo, M.E. Baran, "*A method to detect high impedance faults in distribution feeders,*" IEEE/PES Transmission & Distribution Conference & Exposition (T&D), 2014.

[32] Daqing Hou, N. Fischer, "*Deterministic High-Impedance Fault Detection and Phase Selection on Ungrounded Distribution Systems,*" Power Systems Conference: Advanced Metering, Protection, Control, Communication, and Distributed Resources, 2006.

[33] H.F. Zhang, Z.C. Pan, Z.G. Tian, "*Detection and Location of Ground Faults Using a Discernible Signal,*" IEEE/PES Transmission and Distribution Conference and Exhibition: Asia and Pacific, 2005.

[34] Matthieu Loos et al., *Detection of Single Phase Earth Fault in Compensated Network with C0 Estimation*, 22nd International Conference on Electricity Distribution (CIRED), 2013.

[35] H. Laaksonen, P. Hovila, "*Straightforward Detection Method for High-Impedance Faults,*" International Review of Electrical Engineering (I.R.E.E.), vol. 12, n. 2, March – April 2017.

[36] A. R. Sedighi, M. R. Haghifam, "Simulation of High Impedance Ground Fault In Electrical Power Distribution Systems," International Conference on Power System Technology, 2010.

[37] Y. Sheng, S.M. Rovnyak, "Decision Tree-Based Methodology for High Impedance Fault Detection" Power Delivery, IEEE Transactions on, Vol.19, Issue: 2, pp.533 – 536, April 2004.

[38] M. Öhrström, "*Fast fault detection for power distribution systems,*" Thesis, Royal Institute of Technology, Stockholm, 2003

[39] Peter Imris, *Transient Based Earth Fault Location in 110 kV Sub-transmission Networks*, Helsinki University of Technology, Department of Electrical and Communications Engineering, Power Systems and High Voltage Engineering, 2006.

Carlos Gonzalez received the Industrial Engineer degree in electrotechnics from Polytechnic University of Catalonia (UPC, Barcelona Tech, Spain) in 2009. From 2006 till 2010, he was researcher at CITCEA-UPC and IREC, Spain. He obtained PhD degree in engineering science (Electrical Department) in 2015, from KU Leuven, Belgium. His research interests include power quality in smart grids and fault detection both in AC and DC distribution grids.

Jeroen Tant (S'08 - M'17) received the M.Sc. degree in Electrical Engineering from the University College Howest, Kortrijk, Belgium, in 2007 and the M.Sc. degree in Mathematical Engineering from the KU Leuven, Leuven, Belgium, in 2009. He received the Ph.D. degree in Electrical Engineering, also from KU Leuven, in 2017. He held a Ph.D. fellowship from the Research Foundation Flanders (FWO). He is currently working as a postdoctoral researcher at KU Leuven. His research topics include the modeling and simulation of power electronic circuits and systems.

Jean Gardy Germain received the M. Eng. degree in Electromecanics from Faculty of Sciences (Haiti) and Institut Grenoble Institute of Technology, France, in 1991, and M.Sc in Economy and Engineering of Energy form Institute of Energy Economics (IDEE-Bariloche Foundation) in 1993 and PhD in Electrical Engineer form Polytechnic University of Madrid, Spain, in 2002. He joined the I+D department of the DSO Gas Natural Fenosa in RST. He has launched several research and demonstration projects in close collaboration with industrial partners. Moreover, since 2003, he is Associate Professor in Power to Gas and Electric Vehicle, European University and Carlos III University of Madrid. He has published more than 20 papers at international conferences (IEE, CIGRÉ and IEEE). He has participated in more than 20 research projects as a Research Engineer. His research interests include transformer condition monitoring, power quality problems and solutions in distribution grids, and applied research to distribution grids.

Tom De Rybel received the Industrial Engineer degree in electronics design from Hogeschool Gent, Belgium, in 2002 and the M.A.Sc and PhD degrees in power systems from the University of British Columbia, Vancouver, Canada, in 2005 and 2010, respectively. His research interests, as a post-doctoral fellow at KU Leuven, Belgium, include smart-grid component design, high-voltage instrumentation, asset condition monitoring, power electronics, acoustics, and hardware-in-the-loop simulation.

Johan Driesen (S93 – M97 SM12) received the M.Sc. and PhD degrees in Electrical Engineering from the Katholieke Universiteit Leuven (KU Leuven), Leuven, Belgium, in 1996 and 2000, respectively. Currently, he is a Professor with the KU Leuven and teaches power electronics and electric drives. In 2000 he was with the Imperial College of Science, Technology and Medicine, London, U.K. In 2002, he was with the University of California, Berkeley. Currently, he conducts research on distributed generation, power electronics, and its applications.